

## CHAPTER 22

# Longitudinal Control Model

A simple yet efficient traffic flow model, in particular one that describes vehicle longitudinal operational control and further characterizes the traffic flow fundamental diagram, is always desirable. Though many models have been proposed in the past, with each having its merits, research in this area is far from conclusive. This chapter introduces a new model—that is, the longitudinal control model (LCM)—with a unique set of properties to the arsenal. The model is suited for a variety of transportation applications, among which a concrete example is provided.<sup>1</sup>

### 22.1 INTRODUCTION

A simple yet efficient traffic flow model, in particular one that describes vehicle longitudinal operational control and further characterizes the traffic flow fundamental diagram, is always desirable. For example, researchers can use such a model to study traffic flow phenomena, system analysts need the model to predict system utilization and congestion, accident investigators find the model handy to reconstruct accidents, software developers may implement the model to enable computerized simulation, and practitioners can devise strategies to improve traffic flow using such a simulation package.

Research has resulted in many traffic flow models, including microscopic car-following models and macroscopic steady-state models, each of which has its merits and is applicable in a certain context with varying constraints. An overview of these historical efforts will be provided in [Section 22.6](#). Nevertheless, research on traffic flow modeling is far from conclusive, and there is a constant quest for better models. Joining such a journey, this chapter presents a new model, the LCM, as a result of modeling from a combined perspective of physics and human factors ([Section 22.2](#)). The model seems to possess a unique set of properties:

- The model is *physically meaningful* because it captures the essentials of longitudinal vehicle control and motion on roadways with the presence of other vehicles ([Subsection 22.2.1](#))

<sup>1</sup> This chapter is reproduced from [113].

- The model is *simple* because it uses one equation to handle all driving situations in the longitudinal direction (Equation 22.2), and this microscopic equation aggregates to a steady-state macroscopic equivalent that characterizes the traffic stream in the entire density range (Equation 22.5).
- The model is *flexible* because the microscopic equation provides the mechanism to admit different safety rules that govern vehicle driving (Section 22.2.1), and the macroscopic equation has the flexibility to fit empirical traffic flow data from a variety of sources which exhibit varying flow-density relationships, including an reverse-lambda type (Section 22.3.2 and Figures 22.3–22.8).
- The model is *consistent* because the microscopic equation aggregates to its macroscopic equivalent, so the microscopic-macroscopic coupling is well defined (Section 22.2.2). As a result, traffic flow modeling and simulation based on the microscopic model aggregates to predictable macroscopic behavior (Section 22.5; see how the results of the microscopic and macroscopic approaches match).
- The model is *valid* as verified by field observations from a variety of locations (Section 22.4), and the model is realistic as demonstrated in an example application (Section 22.5).

The unique set of properties possessed by the LCM lend it to various transportation applications, including those mentioned above. An example of such applications is described in Section 22.5, where the LCM is applied to analyze traffic congestion macroscopically and microscopically. Research findings are summed up in Section 22.7.

## 22.2 THE LCM

Vehicle operational control in the longitudinal direction concerns a driver's response in terms of acceleration and deceleration on a highway without the worrying about steering, including lane changing. Rather than car following as it is conventionally termed, vehicle longitudinal control involves more driving regimes than simply car following (e.g., free flow, approaching, stopping). A field theory was proposed in Refs. [114, 115], and represents the environment (e.g., the roadway and other vehicles) perceived by a driver with ID  $i$  as an overall field  $U_i$ . As such, the driver is subject to forces as a result of the field. These forces, which impinge upon the driver's mentality, are the driving force  $G_i$ , roadway resistance  $R_i$ , and vehicle interaction  $F_i^j$  with the leading vehicle  $j$  (see Figure 22.1). Hence, the driver's response is

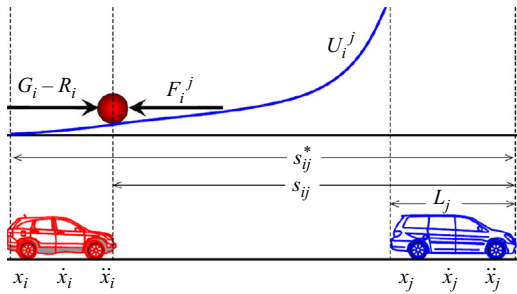


**Figure 22.1** Forces acting on a vehicle.

the result of the net force  $\sum F_i$  acting on the vehicle according to Newton's second law of motion:

$$\sum F_i = G_i - R_i - F_i^j. \quad (22.1)$$

### 22.2.1 Microscopic Model

If the functional forms of the terms in Equation 22.1 are carefully chosen (mainly by experimentation with empirical data), a special case called the LCM can be explicitly derived from Equation 22.1 as

$$\ddot{x}_i(t + \tau_i) = A_i \left[ 1 - \left( \frac{\dot{x}_i(t)}{v_i} \right) - e^{1 - \frac{s_{ij}(t)}{s_{ij}^*(t)}} \right], \quad (22.2)$$

where  $\ddot{x}_i(t + \tau_i)$  is the operational control (acceleration or deceleration) of driver  $i$  executed after a perception-reaction time  $\tau_i$  from the current moment  $t$ .  $A_i$  is the maximum acceleration desired by driver  $i$  when starting from standing still,  $\dot{x}_i$  is vehicle  $i$ 's speed,  $v_i$  is driver  $i$ 's desired speed,  $s_{ij}$  is the actual spacing between vehicle  $i$  and its leading vehicle  $j$ , and  $s_{ij}^*$  is the desired value of  $s_{ij}$ .

No further motivation for this special case is provided other than the following claims: (1) it takes a simple functional form that involves physically meaningful parameters but not arbitrary coefficients (see this and the next section), (2) it makes physical and empirical sense (see this section and Section 22.4), (3) it provides a sound microscopic basis for aggregated behavior—that is, traffic stream modeling (see the remainder of this section and Section 22.4)—and (4) it is simple and easy to apply (see Section 22.5).

The determination of the desired spacing  $s_{ij}^*(t)$  admits safety rules. Basically, any safety rule that relates spacing to the driver's speed choice can

be inserted here. Of particular interest is an algorithm for the desired spacing that allows vehicle  $i$  to stop behind its leading vehicle  $j$  after a perception-reaction time  $\tau_i$  and a deceleration process (at rate  $b_i > 0$  which driver  $i$  believes that he or she is capable of applying in an emergency) should the leading vehicle  $j$  apply an emergency brake (at rate  $B_j > 0$ ). After some math, the desired spacing can be determined as

$$s_{ij}^*(t) = \frac{\dot{x}_i^2(t)}{2b_i} - \frac{\dot{x}_j^2(t)}{2B_j} + \dot{x}_i\tau_i + l_j, \quad (22.3)$$

where  $s_{ij}^* \geq l_j$  and  $l_j$  is vehicle  $j$ 's effective length (i.e., actual vehicle length plus some buffer spaces at both ends). Note that the term  $\frac{\dot{x}_i^2(t)}{2b_i} - \frac{\dot{x}_j^2(t)}{2B_j}$  represents the degree of aggressiveness that driver  $i$  chooses. For example, when the two vehicles travel at the same speed, this term becomes  $\gamma_i \dot{x}_i^2$ , where

$$\gamma_i = \frac{1}{2} \left( \frac{1}{b_i} - \frac{1}{B_j} \right), \quad (22.4)$$

where  $B_j$  represents driver  $i$ 's estimate of the emergency deceleration which is most likely to be applied by driver  $j$ , while  $b_i$  is the deceleration which driver  $i$  believes that he or she is capable of applying in an emergency. It may be that  $b_i$  is greater than  $B_j$  in magnitude, which translates to the willingness (or aggressive characteristic) of driver  $i$  to take the risk of tailgating.

It is necessary to point out that though both  $B_j$  and  $b_i$  carry a sense of “emergency,” the model itself (i.e., Equations 22.2 and 22.3) is meant to describe all situations, including both “emergency” and “normal” operations. Or put it in another way, the LCM models a driver’s operational control  $\ddot{x}_i$  over a wide range on the basis of the interaction of a set of parameters, some of which concern the driver’s emergency responses—for example,  $B_j$  and  $b_i$ . This modeling philosophy echoes the “complete” car-following model described in Ref. [116, p. 158].

## 22.2.2 Macroscopic Model

Under steady-state conditions, vehicles in the traffic behave uniformly, and thus their identities can be dropped. Therefore, the microscopic LCM (Equations 22.2 and 22.3) can be aggregated to its macroscopic equivalent (traffic stream model):

$$v = v_f (1 - e^{1 - \frac{k^*}{k}}), \quad (22.5)$$

where  $v$  is traffic space mean speed,  $v_f$  is free-flow speed,  $k$  is traffic density, and  $k^*$  takes the following form:

$$k^* = \frac{1}{s^*} = \frac{1}{\gamma v^2 + \tau v + l}, \quad (22.6)$$

where  $\gamma$  and  $\tau$  denote the aggressiveness and average response time, respectively, that characterize the driver population, and  $l$  denotes the average effective vehicle length. Equivalently, the macroscopic LCM can be expressed as

$$k = \frac{1}{s} = \frac{1}{(\gamma v^2 + \tau v + l)[1 - \ln(1 - \frac{v}{v_f})]}. \quad (22.7)$$

## 22.3 MODEL PROPERTIES

The LCM features a set of appealing properties that make the model unique. Firstly, it is a one-equation model that applies to a wide range of situations. More specifically, the microscopic LCM captures not only the car-following regime, but also other regimes, such as starting up, free flow, approaching, cutting off, and stopping (see Ref. [117] for more details). The macroscopic LCM applies to the entire range of density and speed without the need to identify break points.

Secondly, the LCM makes physical sense since it is rooted in basic principles (such as field theory and Newton's second law of motion). In addition, the LCM employs a set of model parameters that are not only physically meaningful but also easy to calibrate. For example, the microscopic LCM involves desired speed  $v_i$ , perception-reaction time  $\tau_i$ , desired maximum acceleration when starting from standing still  $A_i$ , the deceleration which driver  $i$  believes that he or she is capable of applying in an emergency  $b_i$ , emergency deceleration  $B_j$  by driver  $j$  in front, and effective vehicle length  $l_j$ . The macroscopic LCM includes aggregated parameters, including free-flow speed  $v_f$ , aggressiveness  $\gamma$ , average response time  $\tau$ , and effective vehicle length  $l$ . Data to calibrate the above parameters are either readily available in publications (such as *Motor Trend* and human factors study reports) or can be sampled in the field with reasonable efforts.

Lastly, the LCM is a consistent modeling approach—that is, the macroscopic LCM is derived from its microscopic counterpart when aggregated over vehicles and time. Such microscopic-macroscopic consistency not

only provides macroscopic modeling with a microscopic basis, but also ensures that microscopic modeling aggregates to a predictable macroscopic behavior.

More properties are discussed in the following subsections.

### 22.3.1 Boundary Conditions

The macroscopic LCM has two clearly defined boundary conditions. When density approaches zero ( $k \rightarrow 0$ ), traffic speed approaches the free-flow speed ( $v \rightarrow v_f$ ); when density approaches the jam density ( $k \rightarrow k_j = 1/l$ ), traffic speed approaches zero ( $v \rightarrow 0$ ) (see [Figure 22.9](#)).

One can determine the kinematic wave speed at jam density  $\omega_j$  by finding the first derivative of flow  $q$  with respect to density  $k$  and evaluating the result at  $k = k_j$ . Hence,

$$q = kv = \frac{v}{(\gamma v^2 + \tau v + l)[1 - \ln(1 - \frac{v}{v_f})]}. \quad (22.8)$$

After some math,

$$\frac{dq}{dk} = v - \frac{s}{s'} = v - \frac{(\gamma v^2 + \tau v + l)[1 - \ln(1 - \frac{v}{v_f})]}{(2\gamma v + \tau)[1 - \ln(1 - \frac{v}{v_f})] + (\gamma v^2 + \tau v + l) \left(\frac{1}{v_f - v}\right)}. \quad (22.9)$$

Therefore,  $\omega_j$  can be evaluated as

$$\omega_j = \left. \frac{dq}{dk} \right|_{k=k_j, v=0} = -\frac{l}{\tau + \frac{l}{v_f}}. \quad (22.10)$$

We can find capacity  $q_m$  by first setting Equation [22.9](#) to zero to solve for optimal speed  $v_m$  or optimal density  $k_m$  and then plugging  $v_m$  or  $k_m$  into Equation [22.8](#) to calculate  $q_m$ . However, it appears that an analytical solution of  $(q_m, k_m, v_m)$  is not easy to find, and this is a limitation of the LCM. Fortunately, the problem can be easily addressed numerically.

On another note, the spacing-speed relationship is

$$s = (\gamma v^2 + \tau v + l) \left[ 1 - \ln \left( 1 - \frac{v}{v_f} \right) \right]. \quad (22.11)$$

We can determine the slope of the speed-spacing relationship when traffic is jammed by finding the first derivative of  $v = f(s)$  with respect to spacing  $s$  and evaluating the result at  $s = l$  and  $v = 0$ :

$$\begin{aligned} \left. \frac{dv}{ds} \right|_{s=l, v=0} &= \left. \frac{1}{(2\gamma v + \tau)[1 - \ln(1 - \frac{v}{v_f})] + (\gamma v^2 + \tau v + l) \left( \frac{1}{v_f - v} \right)} \right|_{s=l, v=0} \\ &= \frac{1}{\tau + \frac{l}{v_f}}. \end{aligned} \quad (22.12)$$

### 22.3.2 Model Flexibility

The macroscopic LCM employs four parameters that allow sufficient flexibility to fit data from a wide range of facilities (see the following section for details). As originally noted in Ref. [38] and later in Refs. [118, 119] concavity is a desirable property of the flow-density relationship. This property is empirically evident in field observations from most highway facilities, especially in outer lanes, and the shape of the flow-density relationship looks like a skewed parabola. In addition, some researchers [28, 31, 118–120] have recognized the attractiveness of having a triangular flow-density relationship. Moreover, an reverse-lambda shape was reported in Refs. [121, 122], most likely in the inner lane of freeway facilities. Therefore, a desirable property of a traffic stream model is its flexibility to represent a variety of flow-density shapes ranging from skewed parabola to triangular to reverse lambda.

The shape of the LCM is related to the second derivative of flow with respect to density:

$$\frac{d^2q}{dk^2} = -\frac{s^3 s''}{s'^3}, \quad (22.13)$$

where

$$s' = \frac{ds}{dv} = (2\gamma v + \tau) \left[ 1 - \ln \left( 1 - \frac{v}{v_f} \right) \right] + (\gamma v^2 + \tau v + l) \left( \frac{1}{v_f - v} \right) \quad (22.14)$$

and

$$s'' = \frac{d^2s}{dv^2} = 2\gamma \left[ 1 - \ln \left( 1 - \frac{v}{v_f} \right) \right] + \frac{4\gamma v + 2\tau}{v_f - v} + \frac{\gamma v^2 + \tau v + l}{(v_f - v)^2}. \quad (22.15)$$

Note that  $s$  is always positive, so the shape of the flow-density relationship is determined by the signs of  $s'$  and  $s''$ . If  $s'$  and  $s''$  are both positive,

$d^2q/dk^2$  is negative and the shape of the flow-density relationship is concave. Otherwise, the flow-density relationship may consist of a combination of concave, straight, and convex sections. In particular, it is possible to obtain an almost triangular shape and even an reverse-lambda shape under certain combinations of parameters  $v_f$ ,  $\tau$ ,  $\gamma$ , and  $l$ , among which  $\gamma$  plays a critical role in controlling the shape of the flow-density relationship. For example, when the driver population is not aggressive—that is,  $\gamma \geq 0$ —a concave flow-density relationship results; a moderately aggressive driver population may give rise to an almost triangular shape, and an aggressive driver population could lead to an reverse-lambda flow-density relationship.

The above discussion is further illustrated in Figure 22.2, where a family of fundamental diagrams are generated from the macroscopic LCM with the following parameters:  $v_f = 30 \text{ m/s}$ ,  $k_j = 0.2$  vehicles per meter,  $\tau = 1 \text{ s}$ , and aggressiveness  $\gamma$  ranging from 0 to  $-0.03 \text{ s}^2/\text{m}$ . In the flow-density plot, the lowest curve, exhibiting a skewed parabolic shape, is generated with  $\gamma = 0$ , the second highest curve, showing a nearly triangular shape, is generated with  $\gamma = -0.027$ , and the highest curve, which has an reverse-lambda shape, is generated with  $\gamma = -0.030$ . From the definition

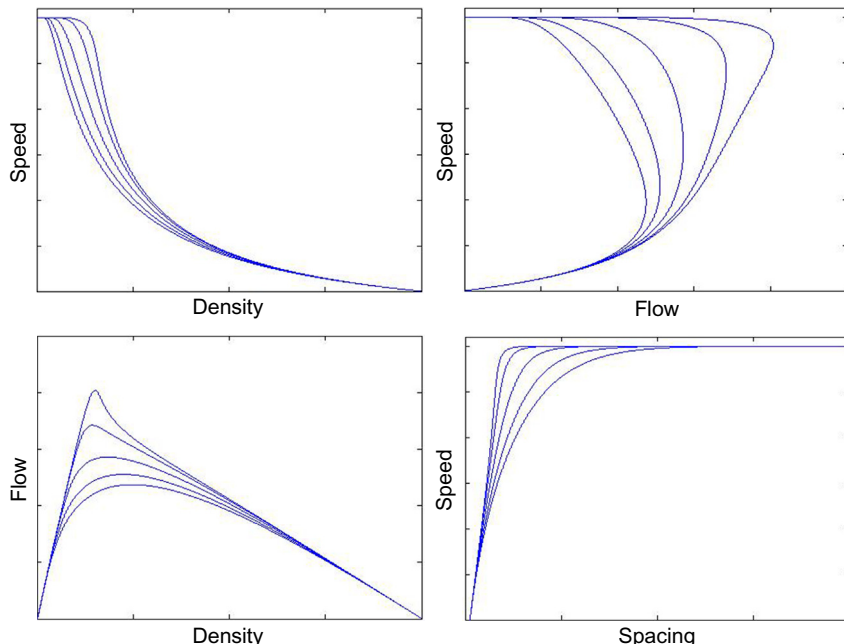


Figure 22.2 Family of curves generated from the LCM with different aggressiveness.

of aggressiveness in Equation 22.4, one recognizes that smaller values of  $\gamma$  correspond to more aggressive drivers, who are willing to accept shorter car-following distances. Therefore, the values of  $\gamma$ , the shape of the  $q - k$  curves, and field observations are consistent. Further quantitative analysis of the effect of aggressiveness and its interaction with other model parameters warrants further research, and is not discussed here.

## 22.4 EMPIRICAL RESULTS

The LCM is tested by fitting the model to traffic flow data collected from a variety of facilities at different locations, including Atlanta (USA), Orlando (USA), Germany, California (USA), Toronto (Canada), and Amsterdam (Netherlands).

Figures 22.3–22.8 illustrate field data observed at these facilities with data “clouds” in the background labeled as “Empirical.” The fitted result of the LCM is illustrated as solid lines labeled as “LCM.” Also shown are the fitted results of other traffic stream models, including the Underwood model [11] (which employs two parameters) and the Newell model [58]

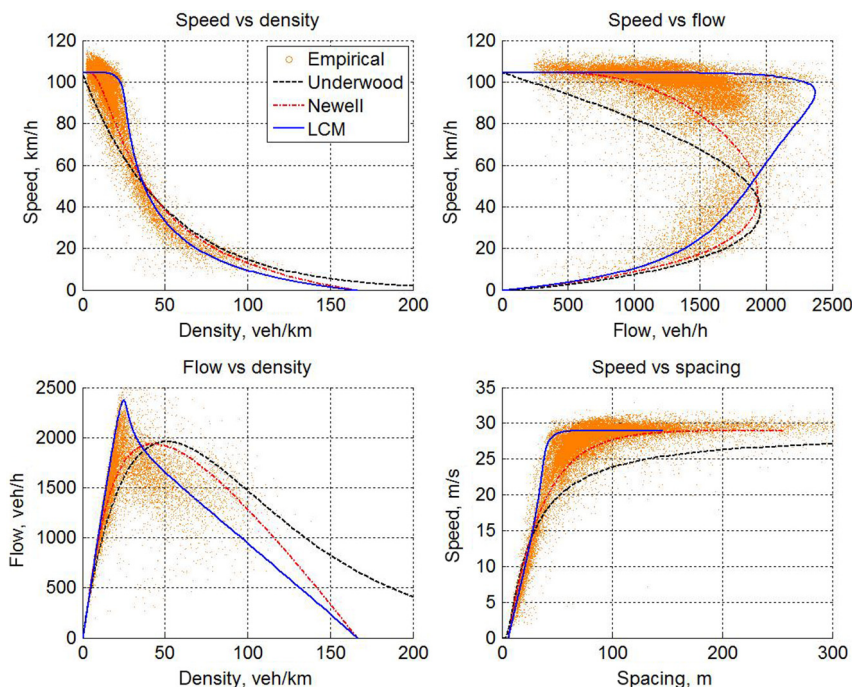
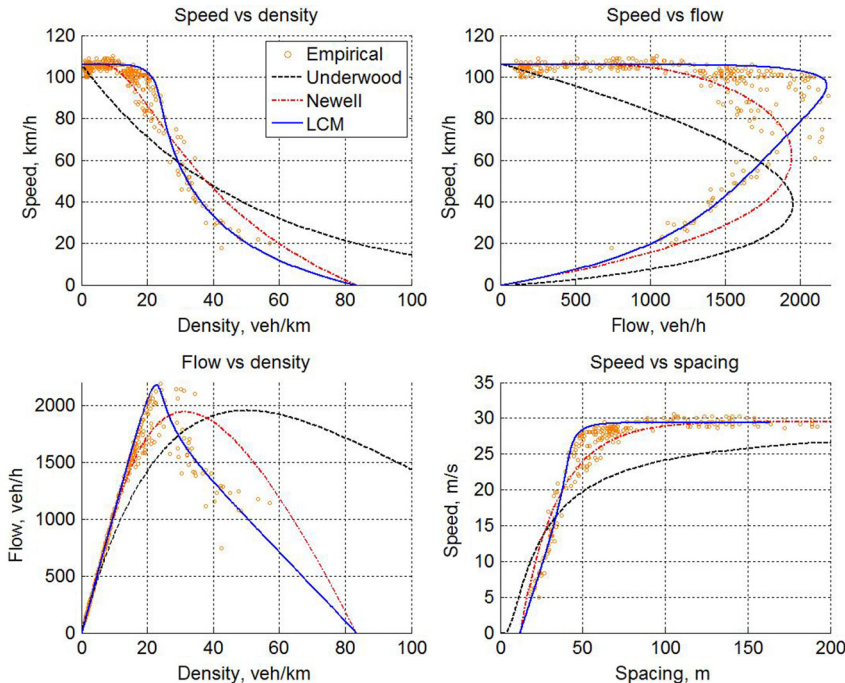


Figure 22.3 LCM fitted to GA400 data.



**Figure 22.4** The LCM fitted to Interstate 4 data.

(three parameters). As such, the reader is able to visually compare the goodness of fit of two-, three-, and four-parameter models and examine how fit quality varies with the number of parameters. Consisting of four plots (namely, speed-density, speed-flow, flow-density, and speed-spacing), each figure illustrates the fundamental diagrams represented by empirical data and these models.

The empirical data in Figure 22.3 were collected on GA400, a toll road in Atlanta, Georgia, USA, at station 4001116. Consisting of 4787 observation points, the abundant field data reveal the relationships among flow, density, and speed by means of cloud density—that is, the intensity of data points. Meanwhile, the wide scatter of the data points seems to suggest that any deterministic, functional fit is merely a rough approximation, and a stochastic approach such as in Ref. [19] might be more statistically sound. By examining the cloud density, one is able to identify the trend of these relationships. For example, the flow-density relationship appears to have an reverse-lambda shape. Meanwhile, the speed-flow relationship features a  $\square$  shape with its “nose” leaning upward.

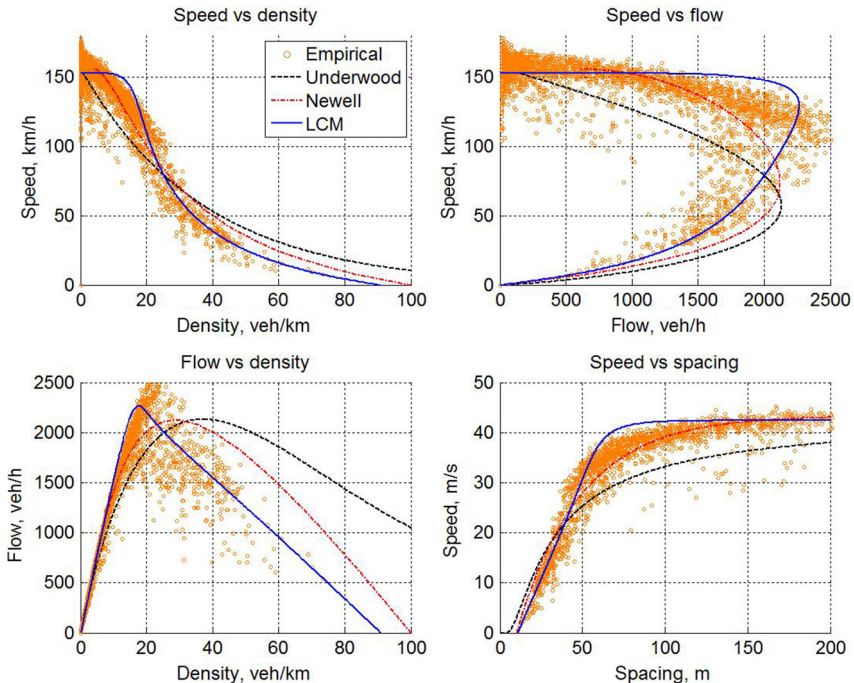


Figure 22.5 LCM fitted to autobahn data.

To fit the LCM to the empirical data, a two-level optimization procedure similar to that in Ref. [123] is adopted. First, each set of raw data is aggregated in order to reduce its size to a manageable level. When the data set is aggregated, its distribution with respect to density is obtained, and the entire density range is divided into intervals delimited by equally spaced quantiles. Then the data are aggregated by computation of an empirical mean (i.e., Emp mean) for each group consisting of the same number of consecutive observations. Next, the two-level optimization procedure is carried out. The inner loop searches for the minimum distance from each dot of “Emp mean” ( $\nu_i$ ,  $k_i$ , and  $q_i$ ) to the LCM curve ( $\hat{\nu}_i$ ,  $\hat{k}_i$ , and  $\hat{q}_i$ ) normalized by ( $\nu_f$ ,  $k_j$ , and  $q_m$ ) given a set of model parameters ( $\nu_f$ ,  $\tau$ ,  $\gamma$ , and  $l$ ):

$$\min d_i = \sqrt{\left(\frac{\nu_i - \hat{\nu}_i}{\nu_f}\right)^2 + \left(\frac{k_i - \hat{k}_i}{k_j}\right)^2 + \left(\frac{q_i - \hat{q}_i}{q_m}\right)^2}. \quad (22.16)$$

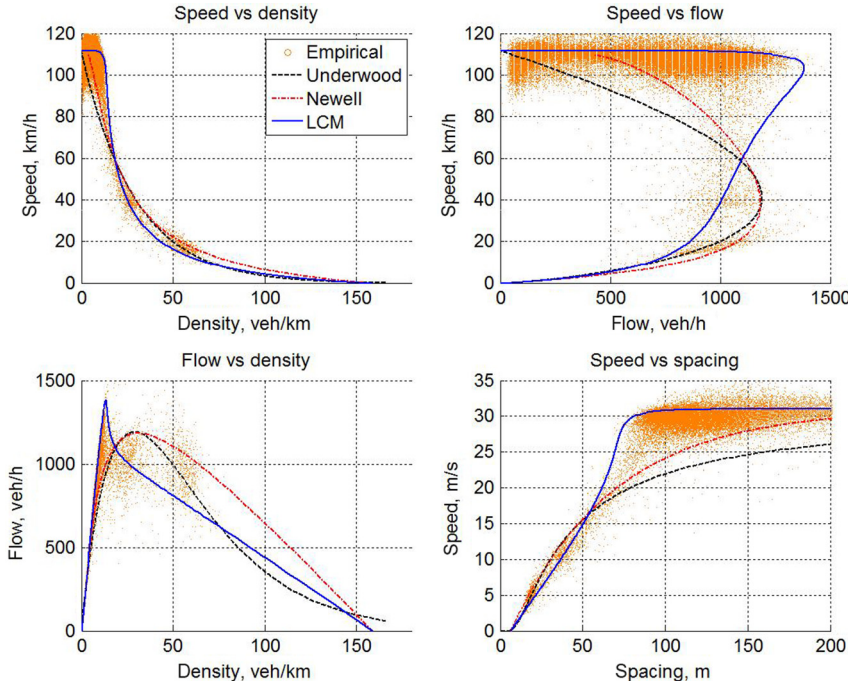


Figure 22.6 The LCM fitted to PeMS data.

Then, the outer loop searches for a set of optimized parameters that minimizes the total of minimized distances  $D(\nu_f, \tau, \gamma, l)$ :

$$\min D = \sum d_i \text{ subject to } \nu_f, \tau, \gamma, \text{ and } l. \quad (22.17)$$

Normally, this would end the fitting process. However, the optimized model does not always match the empirical capacity condition ( $q_m$ ,  $k_m$ , and  $\nu_m$ ) since it consists only of a limited number of observations. If the capacity condition is also part of the fitting objective, one may need to tweak the optimized model, and this is typically done manually by visual inspection.

The fitting results are indicated in Tables 22.1 and 22.2. Table 22.1 compares the fitted capacity condition with the empirical capacity condition. The relative error of capacity is less than 5% and those of optimal density and speed are generally under 10%. Table 22.2 lists fitted parameters of the LCM. For example, the GA400 data set suggests a free-flow speed  $\nu_f$  of 29 m/s (104.4 km/h), an effective vehicle length  $l$  of 6 m (or jam density  $k_j = 167$  vehicles per kilometer), an average response time  $\tau$  of 1.3 s, and

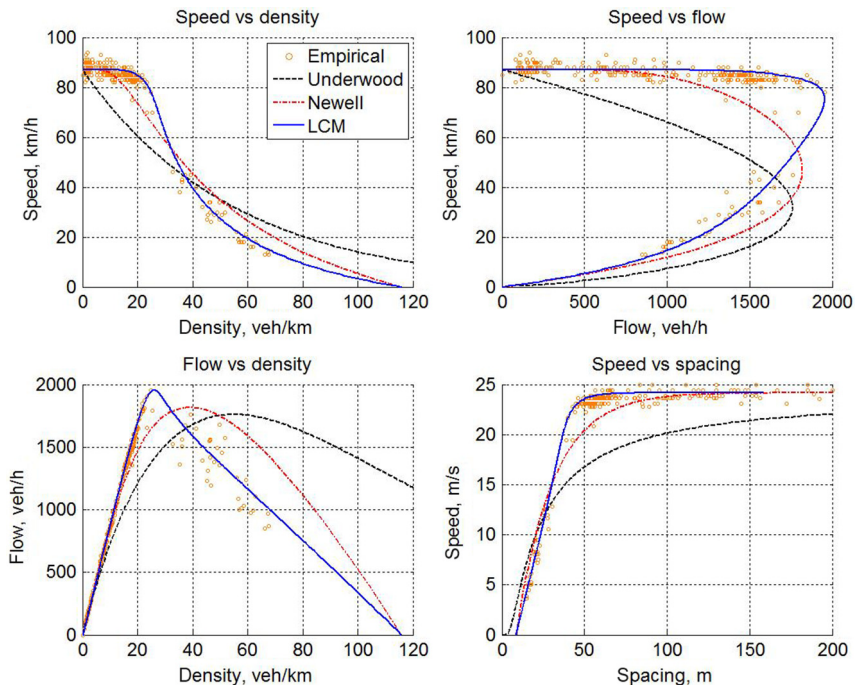


**Figure 22.7** The LCM fitted to Highway 401 data.

aggressiveness  $\gamma$  of  $-0.041 \text{ s}^2/\text{m}$ . In addition, the kinematic wave speed at the jam condition  $\omega_j$  is calculated with Equation 22.10. Though  $\omega_j$  typically lies in a relatively narrow range between 15 and 25 km/h, outliers are observed in field data. For example, the CA/PeMS data set does not provide a clear clue to estimate  $\omega_j$ , while the autobahn data set suggest an  $\omega_j$  of 31.4 km/h or even higher.

We fitted two additional models to the data sets by matching empirical free-flow speed and capacity, and the results are presented in Table 22.2. It is apparent that the more parameters a model employs, the more flexible the model becomes, and hence the more likely it is to result in a good fit. In the speed-flow plot in Figure 22.3, the Underwood and Newell models are comparable in the congested regime (i.e., the lower portion of the graph), while in the free-flow regime (i.e., the upper portion of the graph) the Newell model outperforms the Underwood model since the Newell model is closer to the dense cloud. In contrast, the LCM (which employs four parameters) yields the best fit among the three models, as indicated by the close approximation of the LCM curve to the empirical

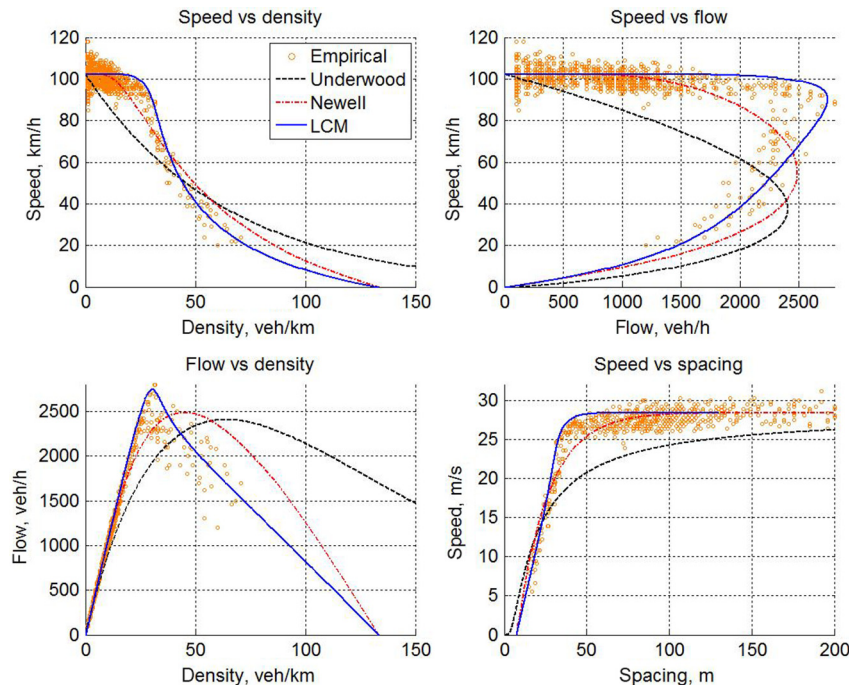


**Figure 22.8** The LCM fitted to Amsterdam data.

data. More specifically, the LCM curve runs through the dense cloud in the free-flow regime and follows the trend nicely in the rest of the graph. In the flow-density plot, both the Underwood model and the Newell model peak later than do the empirical data. In the congested regime (i.e., the portion after the peak), both models exhibit a lack of fit, with the Newell model slightly better in terms of concavity and closeness to data points. In contrast, the LCM is superior on all accounts. Not only does it exhibit an reverse-lambda shape, it is also much closer to the empirical data. In addition, the curve peaks at the same location where the empirical data peak ( $k_m = 25$  vehicles per kilometer). In the speed-density plot, the LCM appears to overfit the data when the density is very low. Except for this, the three models have their own relative merits since each appears to fit the empirical data reasonably well. The speed-spacing plot emphasizes the free-flow regime, which is the flat portion at the top of the graph. It appears that the Underwood model takes a long way to approach free-flow speed, while the Newell model and the LCM adapt to free-flow speed sooner.

**Table 22.1** Parameters of the LCM as a result of fitting to various facility types

Data source		Empirical parameters					Capacity condition		
Location	Facility	No. of observations	$v_f$ (m/s)	$l$ (m)	$\tau$ (s)	$\gamma$ ( $s^2/m$ )	$q_m$ (vehicles/h)	$k_m$ (vehicles/km)	$v_m$ (km/h)
Atlanta	GA400	4787	29.5	4	1.46	-0.038	1883.8	22.0	85.8
Orlando	Interstate 4	288	24.2	8.6	1.09	-0.040	1795.5	22.1	81.4
Germany	Autobahn	3405	43.3	10	1.0	-0.018	2114.1	22.3	95.0
CA/PeMS	Freeway	2576	31	6.3	2.4	-0.060	1124.9	11.0	102.5
Toronto	Highway 401	286	29.5	12	0.8	-0.026	1945.7	21.8	89.2
Amsterdam	Ring road	1199	28.4	7.5	0.82	-0.026	2452.2	27.2	90.3

**Table 22.2** Comparison of traffic stream models fitted to various facility types

<b>Location</b>	<b>Model</b>	<b>Estimated parameters</b>
Atlanta	Underwood	$v_f = 29.5 \text{ m/s}$ , $k_m = 0.050 \text{ vehicles/m}$
	Newell	$v_f = 29.5 \text{ m/s}$ , $l = 4.0 \text{ m}$ , $\lambda = 0.81 \text{ 1/s}$
	LCM	$v_f = 29.5 \text{ m/s}$ , $l = 4.0 \text{ m}$ , $\tau = 1.46 \text{ s}$ , $\gamma = -0.038 \text{ s}^2/\text{m}$
Orlando	Underwood	$v_f = 24.2 \text{ m/s}$ , $k_m = 0.055 \text{ vehicles/m}$
	Newell	$v_f = 24.2 \text{ m/s}$ , $l = 8.6 \text{ m}$ , $\lambda = 1.09 \text{ 1/s}$
	LCM	$v_f = 24.2 \text{ m/s}$ , $l = 8.6 \text{ m}$ , $\tau = 1.09 \text{ s}$ , $\gamma = -0.040 \text{ s}^2/\text{m}$
Germany	Underwood	$v_f = 43.3 \text{ m/s}$ , $k_m = 0.037 \text{ vehicles/m}$
	Newell	$v_f = 43.3 \text{ m/s}$ , $l = 10.0 \text{ m}$ , $\lambda = 1.12 \text{ 1/s}$
	LCM	$v_f = 43.3 \text{ m/s}$ , $l = 10.0 \text{ m}$ , $\tau = 1.00 \text{ s}$ , $\gamma = -0.018 \text{ s}^2/\text{m}$
CA/PeMS	Underwood	$v_f = 31.0 \text{ m/s}$ , $k_m = 0.029 \text{ vehicles/m}$
	Newell	$v_f = 31.0 \text{ m/s}$ , $l = 6.3 \text{ m}$ , $\lambda = 0.50 \text{ 1/s}$
	LCM	$v_f = 31.0 \text{ m/s}$ , $l = 6.3 \text{ m}$ , $\tau = 2.40 \text{ s}$ , $\gamma = -0.060 \text{ s}^2/\text{m}$
Toronto	Underwood	$v_f = 29.5 \text{ m/s}$ , $k_m = 0.050 \text{ vehicles/m}$
	Newell	$v_f = 29.5 \text{ m/s}$ , $l = 12.0 \text{ m}$ , $\lambda = 1.3 \text{ 1/s}$
	LCM	$v_f = 29.5 \text{ m/s}$ , $l = 12.0 \text{ m}$ , $\tau = 0.80 \text{ s}$ , $\gamma = -0.026 \text{ s}^2/\text{m}$
Amsterdam	Underwood	$v_f = 28.4 \text{ m/s}$ , $k_m = 0.064 \text{ vehicles/m}$
	Newell	$v_f = 28.4 \text{ m/s}$ , $l = 7.5 \text{ m}$ , $\lambda = 1.5 \text{ 1/s}$
	LCM	$v_f = 28.4 \text{ m/s}$ , $l = 7.5 \text{ m}$ , $\tau = 0.82 \text{ s}$ , $\gamma = -0.026 \text{ s}^2/\text{m}$

Unfortunately, the congested regime (the slope at the beginning portion of this graph) does not reveal much difference among the three models since they all cluster tightly together.

As shown in [Figure 22.4](#) and [Table 22.1](#), Interstate 4 data in Orlando, Florida, USA, feature a capacity  $q_m$  of 1953 vehicles per hour, which is achieved at an optimal density  $k_m$  of 24.9 vehicles per kilometer and optimal speed  $v_m$  of 78.4 km/h. What is striking in this set of data is that the free-flow regime in the speed-flow plot is almost flat and this condition is sustained almost up to capacity. This graph clearly differentiates the fitting quality of models with different numbers of parameters. More specifically, the two-parameter Underwood model exhibits the poorest fit since its upper branch (i.e., free-flow regime), nose (i.e., capacity), and lower branch (i.e., congested regime) are far from empirical observations. The three-parameter Newell model is better, as indicated by the closer fit of its upper branch, nose, and lower branch. The four-parameter LCM is superior in all aspects. For example, its upper branch is almost a flat line running through empirical data points, its nose leans upward and roughly coincides with empirically observed capacity, and its lower branch cuts evenly through empirical observations. Though there are discrepancies between the empirical data

and the fitted curve, no systematic overfitting or underfitting is observed in this graph. In the remaining three plots, the differences among the three models and their fit quality are consistent with those observed in the speed-flow plot.

In [Figure 22.5](#), the autobahn data collected from Germany exhibit an unusually high free-flow speed  $v_f$  of 42.4 m/s (or 152.6 km/h). Unlike the Interstate 4 data, which feature an almost constant free-flow speed  $v_f$  up to capacity, the traffic speed in the autobahn data gradually decreases in the free-flow regime, resulting in an optimal speed  $v_m$  of only about 60% of  $v_f$  as shown in the speed-flow plot. Unfortunately, the particular nature of this set of data poses a great challenge to any attempt to fit the data. In the speed-flow plot, one has difficulty to fit a model that meets the observed free-flow regime, the congested regime, and the capacity simultaneously, so a trade-off has to be made among the three portions. The LCM curve has been tweaked between free-flow and congested regimes while emphasizing the capacity. Though better than the Underwood and Newell models, the LCM still exhibits some discrepancies compared with the empirical data.

The PeMS data collected from California are plotted in [Figure 22.6](#). This set of data heavily emphasizes the free-flow regime (which is virtually a flat band in the speed-flow plot), with observations elsewhere sparsely scattered. In addition, a remarkable feature in the flow-density plot is the spike at capacity, which clearly indicates an reverse-lambda flow-density relationship. As expected, the LCM is able to be fitted to such a shape, and thus approximates the free-flow regime and the capacity condition very well. Since there are few observations in the congested regime, the model fit in this area appears to be quite arbitrary. In comparison, the LCM approximates the free-flow regime and the capacity condition the best, while the Underwood and Newell models are slanted and significantly underestimate the optimal speed  $v_m$ .

Though field observations on Highway 401 in Toronto do not have abundant data points, a trend is still clearly established in each plot in [Figure 22.7](#). Much like the results for the Interstate 4 data, there are clearly differences in capabilities among the models, with the two-parameter Underwood model being the poorest and the four-parameter model being the best. Notice that no systematic underfitting or overfitting is observed in the LCM curves. The same comments as above apply to ring road data in Amsterdam (see [Figure 22.8](#)).

## 22.5 APPLICATIONS

Since the LCM takes a simple mathematical form that involves physically meaningful parameters, the model can be easily applied to help investigate traffic phenomena at both the microscopic level and the macroscopic level. For illustrative purposes, a concrete example is provided below, in which a moving bottleneck is created by a sluggish truck. Microscopic modeling allows the LCM to generate profiles of vehicle motion so that the cause and effect of vehicles slowing down or speeding up can be analyzed in exhaustive detail; macroscopic modeling may employ the LCM to generate fundamental diagrams that help determine shock paths and develop graphical solutions. Since the LCM is consistent at the microscopic and macroscopic levels, the two sets of solutions not only agree with but also complement each other.

In addition, the LCM can be adopted by existing commercial simulation packages to improve their internal logic of car following, or it can serve as the basis of a new simulation package. Moreover, the LCM can be adopted in highway capacity and level of service analysis. For example, the conventional level of service analysis procedure involves the use of speed-flow curves to determine traffic speed; see Ref. [124] for the family of curves in EXHIBIT 23-3 and the set of approximating equations underneath. The macroscopic LCM can help make the analysis more effective by providing more realistic speed-density curves to facilitate analytical, numerical, and graphical solutions. Furthermore, the LCM can be adopted by transportation planners for use as the basis of a highway performance function which realistically estimates travel time (via traffic speed) as a function of traffic flow assigned to a route. The resultant travel time is the basis of driver route choice behavior, which in turn alters dynamic traffic assignment.

### 22.5.1 An Illustrative Example

A freeway segment contains an on-ramp (which is located 2000 m from an arbitrary reference point denoting the upstream end of the freeway) and an off-ramp 2000 m apart. The freeway was initially operating under condition A (flow 0.3333 vehicles per second or 1200 vehicles per hour, density 0.0111 vehicles per meter or 11.1 vehicles per kilometer, and speed 30 m/s or 108.0 km/h). At 2:30 p.m., a slow truck enters the freeway traveling at a speed of 5.56 m/s (20 km/h), which forces the traffic to operate under condition B (flow 0.3782 vehicles per second or 1361 vehicles per hour,

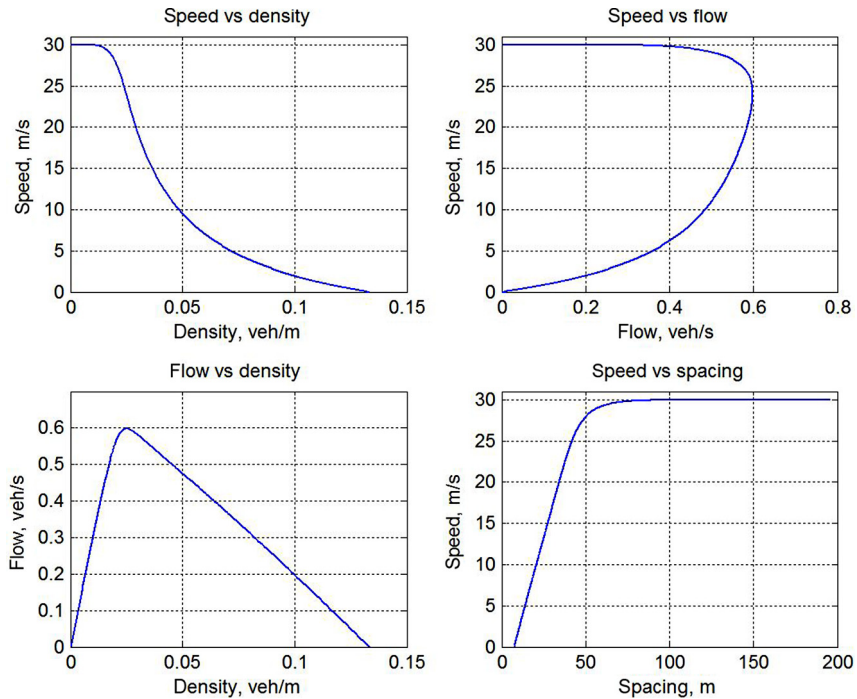


**Figure 22.9** Fundamental diagram of the freeway generated from the LCM.

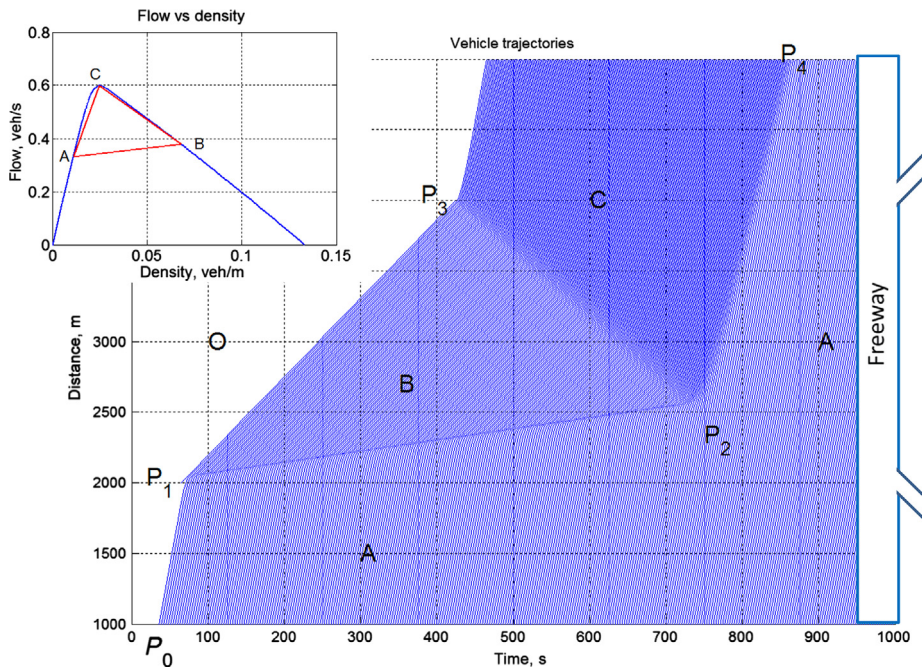
density 0.0681 vehicles per meter or 68.1 vehicles per /kilometer, and speed 5.56 m/s or 20 km/h). After a while, the truck turns off the freeway at the next exit. The impact on the traffic due to the slow truck is illustrated macroscopically in [Section 22.5.2](#) and microscopically in [Sections 22.5.3](#) and [22.5.4](#).

A fundamental diagram, which is illustrated in [Figure 22.9](#), is generated with the macroscopic LCM to characterize the freeway with the following parameters: free-flow speed  $v_f = 30$  m/s, aggressiveness  $\gamma = -0.028 \text{ s}^2/\text{m}$ , average response time  $\tau = 1$  s, and effective vehicle length  $l = 7.5$  m. In addition, the above-mentioned traffic flow conditions, free-flow condition O, and capacity condition C are tabulated in [Table 22.3](#).

To illustrate the application of the LCM, the above problem is addressed in two approaches: a macroscopic graphical solution and a microscopic simulation solution. The microscopic simulation is conducted in deterministic and random fashions.

**Table 22.3** Traffic flow conditions

Condition	Flow, $q$ veh/s (veh/h)	Density $k$ veh/m (veh/km)	Speed $v$ m/s (km/h)
A	0.3333 (1200.0)	0.0111 (11.1)	30 (108.0)
B	0.3782 (1361.6)	0.0681 (68.1)	5.56 (20.0)
C	0.5983 (2154.0)	0.0249 (24.9)	24.03 (86.5)
O	0 (0)	0 (0)	30 (108.0)

**Figure 22.10** A moving bottleneck due to a slow truck; deterministic simulation.

### 22.5.2 Macroscopic Approach—Graphical Solution

The graphical solution to the problem involves finding shock paths that delineate time-space ( $t-x$ ) regions of different traffic conditions. Figure 22.10 illustrates the time-space plane with the freeway overlaid on the right and a mini version of the flow-density plot in the top-left corner. The point when the slow truck enters the freeway (2:30 p.m.) roughly corresponds to  $P_1(t_1 = 65, x_1 = 2000)$  on the time-space plane, while the point when the truck turns off the freeway is roughly  $P_3(t_3 = 425, x_3 = 4000)$ . Therefore, constrained by the truck, the  $t-x$  region under  $P_1P_3$  should contain traffic

condition B. On the other hand, the  $t$ - $x$  regions before the truck enters the freeway and before congestion occurs (i.e., condition B) should have condition A. As such, there must be a shock path that delineates the two regions, and such a path should start at  $P_1$  with a slope equal to shock wave speed  $U_{AB}$ , which can be determined according to Rankine–Hugoniot jump condition [125, 126]:

$$U_{AB} = \frac{q_B - q_A}{k_B - k_A} = \frac{0.3782 - 0.3333}{0.0681 - 0.0111} = 0.7877 \text{ m/s.} \quad (22.18)$$

Meanwhile, downstream of the off-ramp, congested traffic departs at capacity condition C, which corresponds to a  $t$ - $x$  region that starts at  $P_3$  and extends forward in time and space. Hence, a shock path forms between the region with condition C and the region with condition B. Such a shock path starts at  $P_3$  and runs with a slope equal to shock wave speed  $U_{BC}$ :

$$U_{BC} = \frac{q_C - q_B}{k_C - k_B} = \frac{0.5983 - 0.3782}{0.0249 - 0.0681} = -5.0949 \text{ m/s.} \quad (22.19)$$

If the flow-density plot is properly scaled, one should be able to construct the above shock paths in the  $t$ - $x$  plane. The two shock paths should eventually meet at point  $P_2(t_2, x_2)$ . Its location can be found by solving the following set of equations:

$$\begin{cases} x_2 - x_1 &= U_{AB} \times (t_2 - t_1), \\ x_2 - x_3 &= U_{BC} \times (t_2 - t_3), \\ (x_2 - x_1) + (x_3 - x_2) &= 2000. \end{cases} \quad (22.20)$$

After some math,  $P_2$  is determined roughly at (716.8, 2513.4). After the two shock paths  $P_1P_2$  and  $P_3P_2$  meet, they both terminate and a new shock path forms which delineates regions with conditions C and A. The slope of the shock path should be equal to shock speed  $U_{AC}$ :

$$U_{AC} = \frac{q_C - q_A}{k_C - k_A} = \frac{0.5983 - 0.3333}{0.0249 - 0.0111} = 19.2029 \text{ m/s.} \quad (22.21)$$

As such, the shock path can be constructed as  $P_2P_4$ . Lastly, the blank area in the  $t$ - $x$  plane denotes a region with no traffic—that is, condition O.

### 22.5.3 Microscopic Approach—Deterministic Simulation

To double check the LCM and to verify if its macroscopic and microscopic solutions agree with each other reasonably, the microscopic LCM is implemented in MATLAB, a computational software package. As a manageable

starting point, the microscopic simulation is made deterministic with the following parameters: desired speed  $v_i = 30 \text{ m/s}$ , maximum acceleration  $A_i = 4 \text{ m/s}^2$ , emergency deceleration  $B_i = 6 \text{ m/s}^2$ , the deceleration which driver  $i$  believes that he or she is capable of applying in an emergency  $b_i = 9 \text{ m/s}^2$ , perception-reaction time  $\tau_i = 1 \text{ s}$ , and effective vehicle length  $l_i = 7.5 \text{ m}$ , where  $i \in \{1, 2, 3, \dots, n\}$  are unique vehicle identifiers. Vehicles arrive at the upstream end of the freeway at a rate of one vehicle every 3 s, which corresponds to a flow of  $q = 1200$  vehicles per hour. The simulation time increment is 1 s and the simulation duration is 1000 s.

[Figure 22.10](#) illustrates the simulation result in which vehicle trajectories are plotted in the  $t$ - $x$  plane. The varying density of trajectories outlines a few regions with clearly visible boundaries. The motion or trajectory of the first vehicle is predetermined, while those of the remaining vehicles are determined by the LCM. The first vehicle enters the freeway at time  $t = 65 \text{ s}$  (2:30 p.m.) after the simulation starts. This moment is calculated so that the second vehicle is about to arrive at the on-ramp at this particular moment. Hence, the second vehicle and vehicles thereafter have to adopt the speed of the truck, forming a congested region where traffic operates at condition B.

Upstream of this congested region B is a region where traffic arrives according to condition A. The interface of regions B and A,  $P_1P_2$ , denotes a shock path in which vehicles in fast platoon A catch up with and join slow platoon B ahead. The situation continues, and the queue keeps growing until the truck turns off the freeway at  $t = 425 \text{ s}$  into the simulation (2:36 p.m.). After that, vehicles at the head of the queue begin to accelerate according to the LCM—that is, traffic begins to discharge at capacity condition C. Therefore, the front of the queue shrinks, leaving a shock path  $P_3P_2$  that separates region C from region B. Since the queue front shrinks faster than the growth of the queue tail, the former eventually catches up with the latter at  $P_2$ , at which point both shock paths terminate, denoting the end of congestion. After the congestion disappears, the impact of the slow truck still remains because it leaves a capacity flow C in front, followed by a lighter and faster flow with condition A. Hence, the trace where faster vehicles in platoon A join platoon C denotes a new shock path  $P_2P_4$ .

Comparison of the macroscopic graphical solution and the microscopic deterministic simulation reveals that they agree with each other very well, though the microscopic simulation contains much more information about the motion of each individual vehicle and the temporal-spatial formation and dissipation of congestion.

## 22.5.4 Microscopic Approach—Random Simulation

Since the microscopic approach allows one the luxury to account for randomness in drivers and traffic flow, the following simulation may replicate the originally posed problem more realistically. The randomness of the above example is set up as follows with the choice of distribution forms being rather arbitrary provided that they are convenient and reasonable:

- Traffic arrival follows a Poisson distribution, in which the headway between the arrival of consecutive vehicles is exponentially distributed with mean 3 s—that is,  $h_i \sim \text{Exponential}(3)s$ , which corresponds to a flow of 1200 vehicles per hour.
- The desired speed follows a normal distribution:  $v_i \sim N(30, 2) \text{ m/s}$ .
- The maximum acceleration follows a triangular distribution:  $A_i \sim \text{Triangular}(3, 5, 4) \text{ m/s}^2$ .
- Emergency deceleration  $B_i \sim \text{Triangular}(5, 7, 6) \text{ m/s}^2$ .
- The deceleration which driver  $i$  believes that he or she is capable of applying in an emergency  $b_i \sim \text{Triangular}(8, 10, 9) \text{ m/s}^2$ .
- Effective vehicle length  $l_i \sim \text{Triangular}(5.5, 9.5, 7.5) \text{ m}$ .

The result of one random simulation run is illustrated in [Figure 22.11](#), where the effect of randomness is clearly observable. Trajectories in region B seem to exhibit the least randomness because vehicles tend to behave uniformly under congestion. Trajectories in region C are somewhat random since the metering effect due to the congestion still remains. In contrast, region A appears to have the most randomness, not only because of the Poisson arrival pattern but also because of the random characteristics of drivers. Consequently, the shock path between regions B and C,  $P_3P_2$ , remains almost unaltered, while there are some noticeable changes in shock path  $P_1P_2$ . The first is the roughness of the shock path, and this is because vehicles in platoon A now join the tail of the queue in a random fashion. The second is that the path might not be a straight line. The beginning part of the shock path has a slope roughly equal to  $U_{AB}$ , while the rest has a slightly steeper slope (due to less intense arrival from the upstream part of the freeway during this period), resulting in the termination of congestion earlier than in the deterministic case (which is somewhere near  $P_2$ ). This, in turn, causes the slope of the shock path between regions C and A to shift left. The slope of this shock path remains nearly the same since this scenario features a fast platoon that is caught by an even faster platoon.

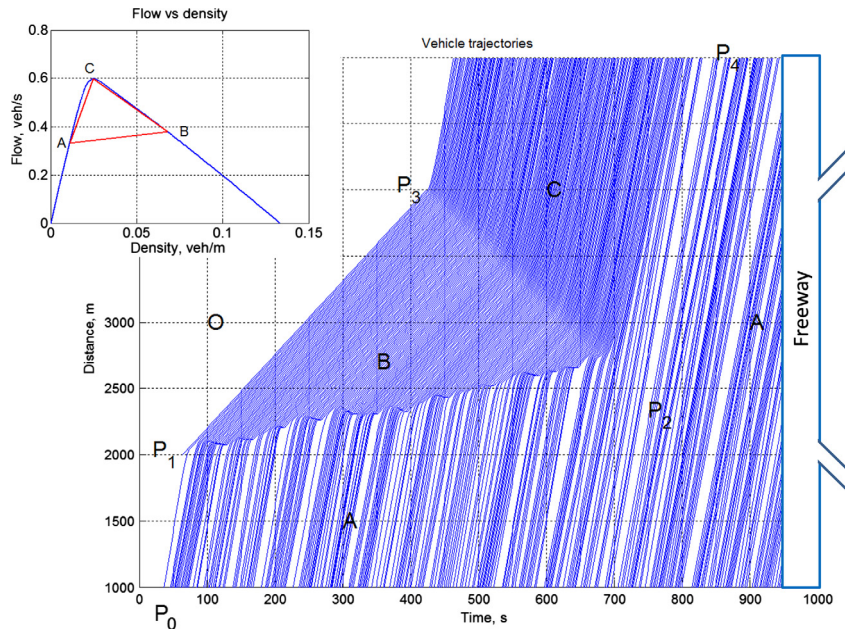


**Figure 22.11** A moving bottleneck due to a slow truck; random simulation.

## 22.6 RELATED WORK

The microscopic LCM is a dynamic model which stipulates the desired motion (or acceleration) of a vehicle as the result of the overall field perceived by the driver. Other examples of dynamic models are General motors models [55, 56] and the intelligent driver model [60, 61, 116]. A dynamic model may reduce to a steady-state model when vehicle acceleration becomes zero. A steady-state model essentially represents a safety rule—that is, the driver's choice of speed as a result of allowing a safe car-following distance or vice versa. Examples of steady-state models include the Pipes model [52], the Forbes model [53, 54, 66], the Newell nonlinear car-following model [58], the Gipps car-following model [57], and the Van Aerde car-following model [62, 63]. Interested readers are referred to [127] for a detailed discussion of the relation among the LCM and other car-following models, including a unified diagram that summarizes such a relation.

The microscopic LCM incorporates a term called the desired spacing  $s_{ij}^*$  (Equation 22.2) which generally admits any safety rule and consequently any

steady-state model. However, Equation 22.3 instantiates  $s_{ij}^*$  in a quadratic form as a simplified version of the Gipps car-following model [57]. The result coincides with the speed-spacing relationship documented in the *Highway Capacity Manual* [128] and Chapter 4 of *Revised Monograph of Traffic Flow Theory* [3] as a result of 23 observational studies. The speed-spacing relationship incorporates three terms: a constant term representing effective vehicle length; a first-order term, which is the distance traveled during perception-reaction time  $\tau$ ; a second-order term, which is the difference of the breaking distances of the following and leading vehicles, and which is interpreted as the degree of aggressiveness that the following driver desires to have. If one ignores the second-order term, the Pipes model [52] and equivalently the Forbes model [53, 54, 66] result.

The macroscopic model is a single-regime traffic stream (or equilibrium) model with four parameters. Also in the single-regime category, the Van Aerde model [62, 63] and the intelligent driver model [60, 61] employ four parameters, the Newell model [58] and the models of del Castillo [118, 120] have three parameters, and early traffic stream models such as those of Greenshields [9], Greenberg [10], Underwood [11], and Drake et al. [12] necessitate the use of only two parameters, though their flexibility and quality of fitting vary, as illustrated in Section 22.4.

## 22.7 SUMMARY

This chapter introduced a simple yet efficient traffic flow model, the LCM, which is a result of modeling from a combined perspective of physics and human factors. The LCM is formulated in two consistent forms: the microscopic model describes vehicle longitudinal operational control, and the macroscopic model characterizes steady-state traffic flow behavior and further the fundamental diagram.

The LCM was tested by fitting it to empirical data collected at a variety of facility types in different locations, including GA400 in Atlanta (USA), Interstate 4 in Orlando (USA), an autobahn in Germany, PeMS in California, Highway 401 in Toronto, and a ring road in Amsterdam. The wide scatter of these data sets suggests that any deterministic, functional fit is merely a rough approximation, and a stochastic approach might be more statistically sound. Test results support the claim that the LCM has sufficient flexibility to yield quality fits to these data sets, some of which even exhibit reverse-lambda flow-density relationships. Meanwhile, two more models are fitted to the same data sets in order to compare them

with LCM. These models include the two-parameter Underwood model and the three-parameter Newell model. The fitting results reveal that the more parameters a model employs, the more flexible the model becomes, and hence the more potential it has to achieve a good fit. Consistently, the Underwood model yields the poorest goodness of fit, while the Newell model represents an upgrade and the LCM maintains the best fit to empirical data.

The unique set of properties possessed by the LCM lend it to various transportation applications. For example, the LCM can be easily applied to help investigate traffic phenomena. An illustrative example was provided showing how to apply the LCM to the impact of a sluggish truck at both the microscopic level and the macroscopic level. Noticeably, the two sets of solutions agree with and complement each other owing to the consistency of the LCM. In addition, the LCM can be adopted by existing commercial simulation packages to improve their internal logic of car following, or perhaps serve as the basis of a new simulation package. Moreover, the LCM may help make highway capacity and level of service analysis more effective by providing more realistic speed-density curves to facilitate analytical, numerical, and graphical solutions. Furthermore, the LCM can assist in effective transportation planning by providing a better highway performance function that helps determine driver route choice behavior.

## PROBLEMS

1. Vehicle  $i$  has just resumed motion after an emergency stop on the hard shoulder of a freeway. According to the microscopic form of the LCM, how long does it take for the vehicle to bring its speed up to 20 m/s? Assume the parameter values specified [Section 22.5.3](#) apply.
2. After some time, vehicle  $i$  is approaching a leading vehicle  $j$ , at which time vehicle  $i$  is traveling at 25 m/s, vehicle  $j$  is traveling at 20 m/s, and the spacing between the two vehicles is 50 m. Use the LCM and use parameter values specified above to calculate the following under this scenario:
  - a. Driver  $i$ 's desired spacing
  - b. Driver  $i$ 's control decision
  - c. When driver  $i$  executes the control decision
3. Building on the above scenario, at this time a third vehicle  $k$  traveling at 23 m/s on the adjacent lane cuts in halfway between vehicles  $i$  and  $j$ .

Assume the same set of parameters apply to vehicle  $k$  as well. Repeat the tasks in problem 2 for vehicles  $i$  and  $k$ .

4. For the scenario above, if the underlying desired spacing model is replaced by the Forbes model and the parameter values remain the same, how would your answers to the above problem change?
5. Assume that the parameters in the above problem apply and are uniform across all drivers and vehicles, and determine the corresponding macroscopic form of the LCM.
6. Use the above macroscopic form of the LCM to determine the following:
  - a. Kinematic wave speed at jam density
  - b. The slope of the speed-spacing relationship when traffic is jammed.
7. Find the capacity condition of the above macroscopic form of the LCM.
8. A unique feature of the macroscopic LCM is its ability to generate different shapes of flow-density curves by varying parameter values within the same functional model form. Use the above set of parameters as a starting point and tweak parameters of your choice to configure the following types of flow-density curves and indicate your set of parameter values for each curve:
  - a. A skewed parabolic shape
  - b. A triangular shape
  - c. An reverse-lambda shape